

Gate-Controlled Spin-Orbit Quantum Interference Effects in Lateral Transport

J. B. Miller,^{1, 2} D. M. Zumbühl,¹ C. M. Marcus,¹ Y. B. Lyanda-Geller,³
D. Goldhaber-Gordon,^{1, 4} K. Campman,⁵ and A. C. Gossard⁵

¹Department of Physics, Harvard University, Cambridge, Massachusetts 02138

²Division of Engineering and Applied Science, Harvard University, Cambridge, Massachusetts 02138

³Naval Research Laboratory, Washington, D.C. 20375

⁴Department of Physics, Stanford University, Stanford, California 94305

⁵Materials Department, University of California at Santa Barbara, Santa Barbara, California, 93106

In situ control of spin-orbit coupling in coherent transport using a clean GaAs/AlGaAs 2DEG is realized, leading to a gate-tunable crossover from weak localization to antilocalization. The necessary theory of 2D magnetotransport in the presence of spin-orbit coupling beyond the diffusive approximation is developed and used to analyze experimental data. With this theory the Rashba contribution and linear and cubic Dresselhaus contributions to spin-orbit coupling are separately estimated, allowing the angular dependence of spin-orbit precession to be extracted at various gate voltages.

An important component along the path toward realizing quantum “spintronic” devices [1, 2] is a structure that allows manipulation of electron spin without destroying phase coherence. Spin-orbit (SO) coupling has been the focus of recent studies because of its potentially useful role in coherent spin rotators [3], spin interference devices [4], and spin-filters [5]. The mechanisms by which SO coupling affects transport [6, 7, 8, 9] have recently been considered in the context of Aharonov-Bohm (AB) phase and Berry phase [4, 10, 11, 12, 13, 14], underscoring the richness of the underlying physics. The results in this and other recent experiments [15] cannot be explained without considering these AB-like effects.

The conductivity of macroscopic low-dimensional systems shows signatures of quantum interference that depend on applied magnetic field and SO coupling [6, 7, 16, 17, 18]. In particular, constructive (destructive) backscattering associated with time-reversed closed-loop electron trajectories in the absence (presence) of significant SO interaction leads to negative (positive) magnetoresistance effects known as weak localization (antilocalization). Antilocalization is the paradigmatic experimental signature of SO coupling in mesoscopic and macroscopic electronic systems [8].

In this Letter, we demonstrate *in situ* control of SO coupling in a moderately high mobility GaAs/AlGaAs two-dimensional electron gas (2DEG), inducing a crossover from weak localization (WL) to antilocalization (AL) as a function of an applied top-gate voltage (see Fig. 1). Theory beyond the diffusive approximation, which also accounts for AB-like spin quantal phases and spin-relaxation [19], is needed to extract gate-voltage-dependent SO parameters from magnetotransport. This theory will be developed here and used to estimate *separately* the various SO terms (Rashba, linear and cubic Dresselhaus, defined below) over a range of gate voltages, ranging from WL to AL.

Conventional WL theories assume SO times much longer than transport scattering times [6, 7, 12] and

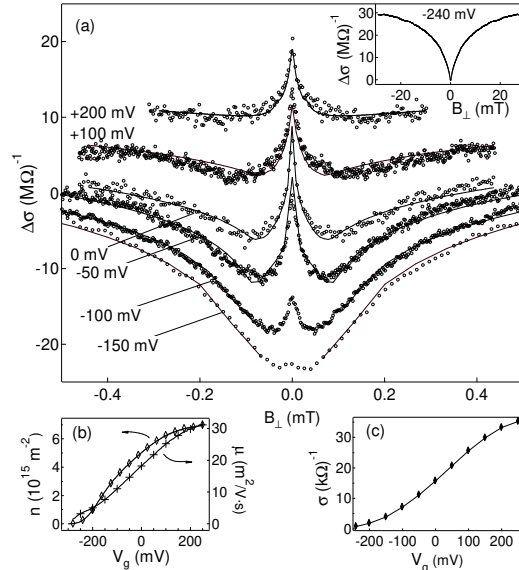


FIG. 1: (a) Experimental magnetoconductance, $\Delta\sigma = \sigma(B) - \sigma(0)$, (circles) offset for clarity, along with three-parameter fits to Eq. (2) (solid curves) for several gate voltages. Inset: Experimental magnetoconductance data for the most negative gate voltage, showing pure WL. (b) Density and mobility as a function of V_g , extracted from longitudinal and Hall voltage measurements. (c) Experimental conductivity, showing strong dependence on V_g . Note that $\Delta\sigma \sim 10^{-3}\sigma$.

so cannot be applied to clean materials such as high-mobility 2DEGs. Previous theories that go beyond the diffusive approximation do not include Rashba and Dresselhaus terms [20, 21, 22] or do so improperly [23].

Previous transport experiments addressing SO phenomena in GaAs heterostructures have investigated relatively disordered samples or weak SO coupling [9, 24], and cleaner materials (without gate control) [25]. Gate-controlled SO coupling has been demonstrated in InGaAs [26, 27, 28], InAs/AlSb [29], HgTe [30] and GaAs 2D hole systems by observing beating patterns seen in Shubnikov-

de Haas oscillations [31, 32], and commensurability oscillations in periodically-modulated 2D structures [33]. The angular variation of SO coupling in GaAs quantum wells has been measured using Raman scattering [34].

The Hamiltonian for conduction band electrons in a [001] 2DEG is $\mathcal{H} = \frac{\hbar^2 k^2}{2m^*} + (\sigma \cdot \Omega)$, where m^* is the effective mass, $\sigma = (\sigma_x, \sigma_y)$ is the Pauli spin operator, and $\Omega = (\Omega_x, \Omega_y)$ is the total SO frequency. Ω can be written as the vector sum of linear (Ω_{D1}) and cubic (Ω_{D3}) Dresselhaus terms and the Rashba term (Ω_R),

$$\Omega_{D1} = \alpha_1 (-\hat{x}\mathbf{k}_x + \hat{y}\mathbf{k}_y) / \hbar, \quad (1a)$$

$$\Omega_R = \alpha_2 (\hat{x}\mathbf{k}_y - \hat{y}\mathbf{k}_x) / \hbar, \quad (1b)$$

$$\Omega_{D3} = \gamma (\hat{x}\mathbf{k}_x \mathbf{k}_y^2 - \hat{y}\mathbf{k}_x^2 \mathbf{k}_y) / \hbar. \quad (1c)$$

where γ is the Dresselhaus coefficient, arising from the lack of inversion symmetry of the GaAs crystal, $\alpha_1 = \gamma \langle k_z^2 \rangle$ is a Dresselhaus parameter that also depends on the thickness of the wavefunction in the quantization direction, and α_2 is the Rashba coefficient, which depends on the potential profile of the heterointerface. The dominant effect of gate voltage, V_g , on Ω is through the carrier density, $n = k^2/2\pi$. Although α_2 can be treated as directly proportional to a *uniform* electric field [35], the magnitude of α_2 in a single-interface heterostructure originates mainly from the band-offset at the heterointerface, which is essentially independent of V_g [29, 36].

The symmetry of the linear (in k) SO terms, Ω_{D1} and Ω_R , allows these terms to be represented as a spin-dependent vector potential \mathbf{A} that affects the orbital motion and phase of electrons, $\sigma \cdot (\Omega_{D1} + \Omega_R) = \mathbf{k} \cdot \mathbf{A}$ [4, 10, 11, 12, 13, 14]. That is, the linear terms affect electronic interference as a spin-dependent AB-like effect. In contrast, the cubic term, Eq. (1c), upon removing terms with the symmetry of Eq. (1a), only causes spin relaxation in the diffusive regime (although it can also produce AB-like effects in the quasi-ballistic regime [4]).

To develop the theory of 2D magnetotransport with SO coupling beyond the diffusive approximation [19], we follow Refs. [20, 21, 22], which treated the quasi-ballistic case without SO coupling, Eq. (1). The approach is to introduce an operator $P = G_{\epsilon+\omega}^R(\mathbf{r}_1, \mathbf{r}_2, \sigma_1)G_{\epsilon}^A(\mathbf{r}_1, \mathbf{r}_2, \sigma_2)\hbar/2\pi\nu\tau$ for the probability of an electron to propagate both forward and backward along a path segment from \mathbf{r}_1 to \mathbf{r}_2 , where G^R (G^A) are single-electron retarded (advanced) Green functions, $\sigma_{1(2)}$ are the Pauli spin operators for particle moving forward (backward), ν is the density of states per spin, and τ is the scattering time. The interference contribution from the n^{th} traversal of a closed path is given by the trace of $(P)^n$. In the presence of SO interactions of the form in Eq. (1), formulas in [22] remain valid once a summation over spins is included in the trace.

Introducing the total spin of interfering partial waves, $\mathbf{S} = \sigma_1 + \sigma_2$, we write $Tr[(P)^n] = \frac{1}{2}Tr[(P_1)^n - (P_0)^n]$,

where operators P_0 and P_1 describe singlet ($\mathbf{S} = \mathbf{0}$) and triplet ($\mathbf{S} = \mathbf{1}$) contributions. To calculate $Tr[(P_{0(1)})^n]$ we find the representations in which $P_{0(1)}$ are diagonal. For SO coupling described by Ω_{D1} and/or Ω_R , these are the representation of the eigenstates of \mathcal{H} for particles with charge $2e$, spin \mathbf{S} and spin frequency 2Ω : $\mathcal{H} = \frac{\hbar^2}{2m^*}(\mathbf{k} - 2e\mathbf{A}_{em} + 2e\mathbf{A}_S)^2$, where \mathbf{A}_{em} is the vector potential associated with the applied perpendicular magnetic field, B , and $\mathbf{A}_S = \frac{m^*}{e\hbar^2}(-\alpha_1 S_x - \alpha_2 S_y, \alpha_2 S_x + \alpha_1 S_y)$ is the SO vector potential. For $\mathbf{S} = \mathbf{0}$, the eigenstates are Landau levels for a charge $2e$ particle in the magnetic field B , analogous to the spinless problem [20]. For $\mathbf{S} = \mathbf{1}$, eigenstates of \mathcal{H} and P_1 in general require a numerical solution, although analytic solutions exist when either α_1 or α_2 equal zero [19]. Here, we find an analytic solution when both α_1, α_2 are nonzero for the case of strong magnetic fields, $L_B < (\ell, L_{so})$, where $L_B = \sqrt{\hbar/2eB}$ is the magnetic length, ℓ is the elastic mean free path, and $L_{so}^{-1} = 2\alpha_{1(2)}m^*/\hbar^2$: performing a unitary transformation $\mathcal{H} \rightarrow \tilde{\mathcal{H}} = U^\dagger \mathcal{H} U$, with $U = \exp(-i\mathbf{A}_S \cdot \mathbf{r})$, and expanding in coordinates, we find $\tilde{\mathcal{H}} = \frac{\hbar^2}{2m^*}(\mathbf{k} - 2e\mathbf{A}_{em} + \mathbf{S}_z \mathbf{a})^2$, where $\mathbf{a} = H_{\text{eff}} \cdot \mathbf{r} \times \hat{z}/2$, and $H_{\text{eff}} = 2(\alpha_2^2 - \alpha_1^2)m^{*2}/e\hbar^3$ is the effective SO field. P_1 can then be block-diagonalized for each m ($m = 0, \pm 1$) using the Landau basis for particles with charge $2e$ in the magnetic field $B - mH_{\text{eff}}$. Thus, the effect of Ω_{D1} and Ω_R is to produce spin quantal phases of the AB type [4, 10, 11, 12, 13, 14]. Higher expansion terms to $\tilde{\mathcal{H}}$ describe spin flip processes and can be taken into account by introducing a spin relaxation time τ_{so} and its corresponding field scale $H_{so} = \hbar\tau/(2e\ell^2\tau_{so})$. The resulting quantum interference contribution takes the form [19]

$$\Delta\sigma(B) = -\frac{e^2}{2\pi^2\hbar} \left[\frac{1}{2} \sum_m C(x_{1m}, f_{1m}) - \frac{1}{2} C(x_{00}, f_{00}) \right] \quad (2)$$

where $x_{Sm} = (B - mH_{\text{eff}})/H_{tr}$ describes the AB dephasing in H_{eff} , $C(y, f_{im}) = y \sum_0^\infty \frac{P_N^3(f_{Sm})}{1 - P_N(f_{Sm})}$, $P_N(f_{Sm}) = s \int_0^\infty \exp(-sf_{Sm}t - t^2/2)dt$, $L_N(t^2)$ and $L_N(z)$ are Laguerre polynomials, $s = (2/|y|)^{1/2}$, and $H_{tr} = \hbar/(2e\ell^2)$. The dephasing factors f_{Sm} are given by $f_{1\pm 1} = (1 + (H_\varphi + H_{so})/H_{tr})$; $f_{00} = (1 + H_\varphi/H_{tr})$; $f_{10} = (1 + (H_\varphi + 2H_{so})/H_{tr})$, where $H_\varphi = \hbar/(4eL_\varphi^2)$, and L_φ is the phase breaking length.

Equation (2) does not include all B -dependent interference terms, notably excluding Cooper-channel contributions due to electron-electron interactions [17] and a reduction of WL due to electron diffraction effects [21]. Also, Eq. (2) is exact only at large B . We find however, that Eq. (2) fits experimental data very well, including at low fields where cubic terms prevent P_1 from being written simply in terms of H_{eff} and H_{so} . In an attempt to capture the effects of cubic terms on

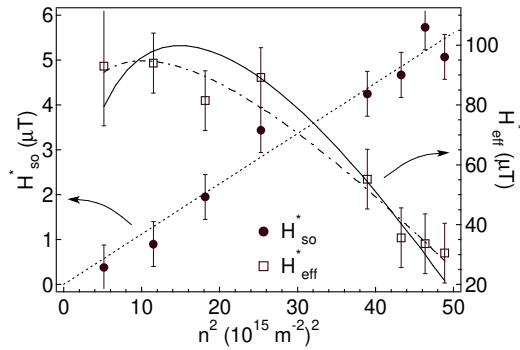


FIG. 2: Spin-orbit effective fields, H_{so}^* (filled circles) and H_{eff}^* (open squares), as extracted using Eq. (2), plotted as a function of sheet density squared. The linear fit to H_{so}^* (dotted line) is used to extract γ . Best fit to H_{eff}^* with γ , α_1 and α_2 as free parameters (dot-dash curve), and holding γ fixed by the value set by the fit to H_{so}^* (solid curve).

H_{eff} and H_{so} , we introduce an effective vector potential $\mathbf{A}_S^* = \mathbf{A}_S + \gamma \frac{m^*}{e\hbar^2} (k_y^2, -k_x^2) \sim \mathbf{A}_S + \gamma \frac{m^*}{2e\hbar^2} (k^2, -k^2)$ which leads to an effective SO field,

$$H_{eff}^* = 2(\alpha_2^2 - \alpha_1^2 + 2\pi n \alpha_1 \gamma - \pi^2 \gamma^2 n^2) m^{*2} / e\hbar^3. \quad (3)$$

Modification of the commutation relation $[\mathbf{k} + \mathbf{A}_S^*, \mathbf{r}]$ by \mathbf{A}_S^* induces spin-flipping terms $\sim \gamma k^3$ in the transformed Hamiltonian \mathcal{H}^* . We estimate the corresponding H_{so}^* using its expression in the diffusive regime, $H_{so}^* = \frac{4}{9} \pi^2 m^{*2} \gamma^2 n^2 / e\hbar$.

We now turn to discuss the experiment. The sample reported here consists of a GaAs/AlGaAs heterostructure grown in the [001] direction with double δ -doping layers set back 143 Å and 161 Å from the 2DEG and a total distance of 346 Å from the surface to the 2DEG. A 200- μ m-wide Hall bar with 700 μ m between voltage probes was patterned by wet etching. A lithographically defined Cr/Au top gate was used to control density and mobility in the Hall bar over the range $n = 1.4\text{--}7.0 \times 10^{15} \text{ m}^{-2}$ and $\mu = 3.6\text{--}31 \text{ m}^2/\text{Vs}$. Measurements were made in a ^3He cryostat at 300 mK using ac lock-in techniques with bias currents ranging from 0.2 to 50 μA (depending on the gate voltage). At each gate voltage, the bias current was experimentally determined not to affect the results. Three samples on two different heterostructures were measured, all showing qualitatively similar behavior.

Figure 1(a) shows the longitudinal magnetoconductance as a function of V_g . A crossover from pure WL (Fig. 1(a), inset) at $V_g = -240 \text{ mV}$ to essentially pure AL at $V_g = +250 \text{ mV}$ is observed. This crossover demonstrates that the gate can be used to control SO over a wide range, as pure WL corresponds to negligible SO rotations within the phase coherence length $L_\varphi(H)$, while AL corresponds to spin rotations $\gtrsim 2\pi$. The solid curves

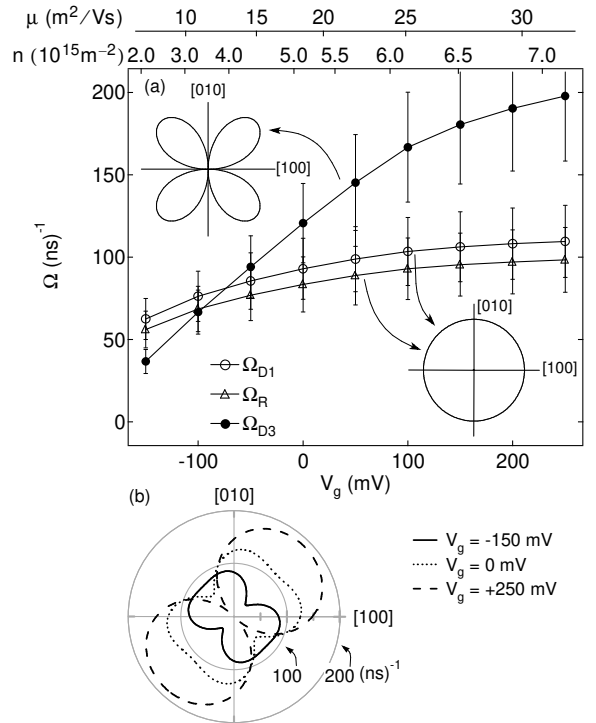


FIG. 3: (a) Magnitudes of isotropic linear Dresselhaus (Ω_{D1}) and Rashba (Ω_R) terms, and nonisotropic cubic Dresselhaus (Ω_{D3}) term as functions of gate voltage, V_g , density, n , and mobility, μ . Insets show dependence on momentum direction for the three terms. Maximum magnitude (when ϕ equals multiples of $\pi/4$) is shown for the anisotropic (Ω_{D3}) term. (b) Angular variation of Ω , the magnitude of the total SO precession vector at $V_g = -150 \text{ mV}$ (solid), 0 mV (dotted), and 250 mV (dashed), corresponding to densities of 2.3, 5.0, and $7.0 \times 10^{15} \text{ m}^{-2}$ respectively.

in Fig. 1(a) are fits of Eq. (2) with three free parameters, H_ϕ , H_{so}^* , and H_{eff}^* . H_{tr} is fixed at each gate voltage by measured values of density and mobility. The entire magnetic field range was used for fitting at all gate voltages except for $V_g = -150 \text{ mV}$ and $V_g = -100 \text{ mV}$, where fitting at low B using Eq. (2) becomes very time consuming.

Figure 2 shows extracted parameters H_{so}^* and H_{eff}^* as a function of n^2 . The density dependence of H_{so}^* is consistent with a linear dependence (dotted line Fig. 2), and a best fit to a straight line gives $\gamma = 28 \pm 2 \text{ eV}\text{\AA}^3$ with zero y-intercept (see Eq. (1c)). Using this γ , the estimates $\alpha_1 = 3.4 \pm 0.5 \text{ meV\AA}$ and $\alpha_2 = 0.31 \pm 0.4 \text{ meV\AA}$ are obtained from the density dependence of H_{eff}^* using Eq. (3) (Fig. 2, solid line). Alternatively, γ can be used as a fitting parameter in Eq. (3) (Fig. 2, dash-dot line), giving values $\gamma = 21 \pm 7 \text{ eV}\text{\AA}^3$, $\alpha_1 = 20 \pm 0.1 \text{ meV\AA}$ and $\alpha_2 = 3 \pm 0.1 \text{ meV\AA}$. In this way, all SO parameters in the Hamiltonian are individually obtained from transport measurements.

Figure 3(a) displays the magnitudes of the three spin-orbit terms as functions of V_g , n , and μ , determined using

Eq. (1) and the extracted values of α_1 , α_2 , and γ from fits to Eq. (2). Plotted are values along the [110] direction, $\phi \equiv \tan^{-1}(\mathbf{k}_y/\mathbf{k}_x) = \frac{\pi}{4}$, where Ω_{D3} is maximum. The error bars indicate uncertainties in the fitting procedure and noise in the data, but do not account for errors due to our model. The angular dependences of the separate Ω terms are shown as insets in Fig. 3(a), indicating that the linear terms are isotropic, while the cubic term has a four-fold symmetry and is highly anisotropic.

The magnitude of the total SO precession frequency Ω as a function of the direction ϕ of the electron momentum is shown for various densities in Fig. 3(b). While for most directions the SO strength is a monotonically increasing function of density, the SO strength along the directions around [110] are seen to decrease with increasing density. This behavior is a result of the different symmetries and relative strengths of the constituent Ω 's. The linear Dresselhaus and Rashba terms (Ω_{D1} and Ω_R) are of comparable magnitude to each other for all densities and in all directions. For ϕ near $\frac{j\pi}{2}$ (j an integer), $\Omega_{D3} \ll \Omega_{D1}, \Omega_R$ and the SO is controlled by the linear terms. For ϕ near $\frac{(2j+1)\pi}{4}$, the cubic term becomes comparable to or even exceeds (at high densities) the linear terms. Depending on ϕ , the linear and cubic terms either add ($\phi \sim \frac{\pi}{4}$) or subtract ($\phi \sim -\frac{\pi}{4}$).

The extracted values for γ , using either H_{so}^* or H_{eff}^* , are in good agreement with the value $27.5 \text{ eV}\text{\AA}^3$ from band structure calculations [26, 36]. Our estimates for α_1 give values for $\langle k_z^2 \rangle$ that correspond to a wavefunction width of $\sim 9\text{-}10 \text{ nm}$ in the perpendicular direction, which is also reasonable. The extracted α_2 corresponds to a uniform [35] electric field $E \sim 6 \text{ MV/m}$, using $\alpha_2 = \alpha_0 e E$ and a value of $\alpha_0 = 5.33 \text{ \AA}^2$ from a $\mathbf{k} \cdot \mathbf{p}$ model [26, 36].

We note that if we had used the previously existing standard WL formulas [7], we would have extracted values for H_{so} that are ~ 5 times higher than those found using Eq. (2). Also, the values for H_{so} obtained in this way would be well fit by a straight line when plotted as a function of n^2 , but the line would not intersect the origin, as seen for instance in Fig. 3 of [9]. Finally, the γ extracted following [7, 12] is $63 \pm 2 \text{ eV}\text{\AA}^3$, which would lead to the unphysical result that $\tau_{so} < \tau$. Following theory in [12, 26] would yield similar unphysical results. We conclude that Refs. [7, 12, 26], which assume the diffusive limit $\ell \ll L_{so}, L_\varphi$, are not applicable to high mobility samples. Our data cannot be fit over a wide range of B if SO is treated only as spin relaxation as in Ref. [23]. A theory for arbitrarily strong SO coupling presented in [13] has also been used to fit this data. Values for Ω_{D3} and Ω_{D1} were estimated using [13] for all V_g 's and agree with our estimates using Eq. (2) to within a factor of $\lesssim 3$. However, the theory in [13] does not separately account for both Ω_{D1} and Ω_R terms, and does not treat magnetic field exactly.

In conclusion, we have realized an *in situ* gate-controlled crossover from weak localization to antilocali-

zation in a GaAs/AlGaAs 2DEG, demonstrating that spin rotation can be modulated in a phase coherent system. New theory addresses spin-orbit effects in the quasi-ballistic regime, allowing separate measurement of Rashba, linear and cubic Dresselhaus terms.

We thank I. Aleiner and H. Bruus for illuminating discussions and F. Mancoff for device fabrication. This work was supported in part by DARPA-QuIST, DARPA-Spins, ARO-MURI, and NSF-NSEC. We also acknowledge support from ONR and NSA (Y. L.-G.), NDSEG (J. B. M.) and the Harvard Society of Fellows (D.G.-G.).

- [1] S. A. Wolf et al., *Science* **294**, 1488 (2001).
- [2] D. D. Awschalom et al., *Semiconductor Spintronics and Quantum Computation* (Springer-Verlag, 2002).
- [3] S. Datta and B. Das, *Appl. Phys. Lett.* **56**, 665 (1990).
- [4] A. G. Aronov and Y. B. Lyanda-Geller, *Phys. Rev. Lett.* **70**, 343 (1993).
- [5] T. Koga et al., *Phys. Rev. Lett.* **88**, 126601 (2002).
- [6] S. Hikami et al., *Prog. Theor. Phys.* **63**, 707 (1980).
- [7] B. Altshuler et al., *JETP* **81**, 788 (1981).
- [8] G. Bergmann, *Phys. Rep.* **107**, 1 (1984).
- [9] P. D. Dresselhaus et al., *Phys. Rev. Lett.* **68**, 106 (1992).
- [10] H. Mathur and A. D. Stone, *Phys. Rev. Lett.* **68**, 2964 (1992).
- [11] Y. B. Lyanda-Geller and A. D. Mirlin, *Phys. Rev. Lett.* **72**, 1894 (1994).
- [12] S. V. Iordanskii et al., *JETP Lett.* **60**, 206 (1994).
- [13] Y. Lyanda-Geller, *Phys. Rev. Lett.* **80**, 4273 (1998).
- [14] I. L. Aleiner and V. I. Fal'ko, *Phys. Rev. Lett.* **87**, 256801 (2001).
- [15] A. F. Morpurgo et al., *Phys. Rev. Lett.* **80**, 1050 (1998).
- [16] E. Abrahams et al., *Phys. Rev. Lett.* **42**, 673 (1979).
- [17] B. L. Altshuler and A. G. Aronov, *Electron-Electron Interactions in Disordered Systems*, ed by A. L. Efros and M. Pollak (North Holland, Amsterdam, 1985), p. 11.
- [18] L. Gorkov et al., *JETP Lett.* **30**, 228 (1979).
- [19] Y. Lyanda-Geller (2002), unpublished.
- [20] A. Kawabata, *J. Phys. Soc. Jpn.* **53**, 3540 (1984).
- [21] V. M. Gasparyan and A. Y. Zyuzin, *Sov. Phys. Solid State* **27**, 999 (1985).
- [22] A. Cassam-Chenai and B. Shapiro, *J. Phys. I* **4**, 1527 (1994).
- [23] A. Zduniak et al., *Phys. Rev. B* **56**, 1996 (1997).
- [24] J. E. Hansen et al., *Phys. Rev. B* **47**, 16040 (1993).
- [25] P. Ramvall et al., *Phys. Rev. B* **55**, 7160 (1997).
- [26] W. Knap et al., *Phys. Rev. B* **53**, 628 (1996).
- [27] J. Nitta et al., *Phys. Rev. Lett.* **78**, 1335 (1997).
- [28] T. Schäpers et al., *J. Appl. Phys.* **83**, 4324 (1998).
- [29] J. P. Heida et al., *Phys. Rev. B* **57**, 11911 (1998).
- [30] M. Schultz et al., *Semicond. Sci. Technol.* **11**, 1168 (1996).
- [31] S. J. Papadakis et al., *Physica E* **9**, 31 (2001).
- [32] R. Winkler et al., *Phys. Rev. B* **65**, 155303 (2002).
- [33] J. P. Lu et al., *Phys. Rev. Lett.* **81**, 1282 (1998).
- [34] B. Jusserand et al., *Phys. Rev. B* **51**, 4707 (1995).
- [35] E. L. Ivchenko and G. E. Pikus, *Superlattices and Other Heterostructures: Symmetry and Optical Phenomena*, vol. 110 of *Springer Series in Solid-State Sciences* (Springer-Verlag, 1995).
- [36] P. Pfeffer, *Phys. Rev. B* **59**, 15902 (1999).